# Experimental and Computational Studies of Alkali-Metal Coinage-Metal Clusters

**Ying-Chan Lin and Dage Sundholm***

*Department of Chemistry, P.O. Box 55 (A.I. Virtanens plats 1), FIN-00014 University of Helsinki, Finland*

**Jonas Jusélius***

*Department of Chemistry, University of Tromsø, N-9037 Tromsø, Norway*

**Li-Feng Cui, Xi Li, Hua-Jin Zhai, and Lai-Sheng Wang***

*Department of Physics, Washington State University, 2710 University Drive, Richland, Washington 99352 and W. R. Wiley Environmental Molecular Sciences Laboratory and Chemical Sciences Division, Pacific Northwest National Laboratory, MS K8-88, P.O. Box 999, Richland, Washington 99352*

*Received: November 23, 2005; In Final Form: February 5, 2006*

Coinage and alkali metal mixed clusters, $M_4Na^-$ (M = Cu, Au) have been investigated experimentally using photoelectron spectroscopy and computationally at correlated ab initio levels. The related $Cu_4Li^-$, $Ag_4Li^-$, $Ag_4Na^-$, and $Au_4Li^-$ clusters as well as the neutral $Cu_4Li_2$ and $Cu_4Na_2$ clusters have also been studied computationally. The calculations show that the two lowest isomers of the negatively charged clusters include a pyramidal $C_{4v}$ structure and a planar $C_{2v}$ species. For $Cu_4Li^-$ and $Cu_4Na^-$, the $C_{4v}$ structure is calculated at correlated ab initio level to be 30.9 and 16.9 kJ/mol below the planar $C_{2v}$ isomer, whereas the planar isomers of $Au_4Li^-$ and $Au_4Na^-$ are found to be 29.7 and 49.4 kJ/mol below the pyramidal ones. For $Ag_4Li^-$ and $Ag_4Na^-$, the pyramidal isomers are the lowest ones. Comparison of the calculated and measured photoelectron spectra of $Cu_4Na^-$ and $Au_4Na^-$ shows that the pyramidal $Cu_4Na^-$ cluster of $C_{4v}$ symmetry and the planar $Au_4Na^-$ of $C_{2v}$ symmetry are detected experimentally. Calculations of the magnetically induced current density in $Cu_4Li^-$ and $Cu_4Li_2$ using the Gauge-Including Magnetically Induced Current (GIMIC) method show that strong ring currents are sustained mainly by the highest-occupied molecular orbital primarily derived from the Cu 4*s*. The GIMIC calculations thus show that the $Cu_4^{2-}$ ring is $\sigma$-aromatic and that the *d* orbitals do not play any significant role for the electron delocalization effects. The present study does not support the notion that the square-planar $Cu_4^{2-}$ is the first example of *d*-orbital aromatic molecules.

## I. Introduction

Photoelectron spectroscopy (PES) and ab initio calculations have recently been used to study a series of ring-shaped metal clusters consisting of planar four-membered molecular rings, which are shown to be stabilized by cyclic electron delocalization or aromaticity.[1−8] The aromatic nature of these ring-shaped metal clusters has been subsequently studied and confirmed.[9−14] The generally accepted notion is that ring-shaped metal clusters with $(4n + 2)\pi$ electrons such as $Al_4^{2-}$ and $Hg_4^{6-}$ can be aromatic and that they sustain ring currents when exposed to external magnetic fields, similar to ordinary aromatic molecules. Explicit calculations of the magnetically induced current densities have shown that for $Al_4^{2-}$, both $\sigma$ and $\pi$ orbitals sustain diatropic (aromatic) ring currents, whereas for $Al_4^{4-}$ species the current is $\sigma$ diatropic (aromatic) and the $\pi$ current is paratropic (antiaromatic). This notion is also supported by earlier calculations of nucleus independent chemical shifts (NICS).[15] Thus, new concepts of multiple aromaticity for metal clusters, such as $\sigma$ and $\pi$ aromaticity, and $\sigma$ aromaticity and $\pi$ antiaromaticity, have been introduced. A recent study of the magnetically induced currents of $Al_4^{2-}$ and $Al_4^{4-}$ using the Gauge-Including Magnetically Induced Current (GIMIC) method[16] yielded explicit values for the ring-current strengths, as well as the diatropic (aromatic) and paratropic (antiaromatic) contributions to the ring current.[14] The ring-current study of the $Al_4$ clusters also provided accurate information about the shape of the magnetically induced ring currents and the aromaticity properties of the controversial case of $Al_4^{4-}$ [17] can now be considered understood:[14] it is $\pi$-antiaromatic and $\sigma$-aromatic as originally suggested.[2]

Wannere et al.[18] recently studied computationally four-membered ring species of coinage metals, such as bipyramidal $Cu_4Li_2$, $Ag_4Li_2$, and $Au_4Li_2$ clusters of $D_{4h}$ symmetry and used NICS calculations to assess their aromaticity. In these cases, Wannere et al.[18] found that the largest diamagnetic (aromatic) contribution to the NICS value originates from the $a_{1g}$ molecular orbital (MO), which is built mainly from the 4*s* atomic orbitals (AOs). However, the paramagnetic (antiaromatic) contribution from the highest occupied $e_u$ orbitals, also formed mainly by the 4*s* AOs, cancels the $a_{1g}$ contribution. Thus, the diamagnetic NICS value of −14.5 ppm seems to originate from the MOs with mainly 3*d* character. They considered therefore these coinage-alkali metal clusters as the first example of *d*-orbital aromatic molecules.[18]

We also mention here the recent density-functional theory (DFT) study by Fuentealba and Padilla-Campos[19] who calculated the molecular structures of neutral and positively charged

* To whom correspondence should be addressed. Email: sundholm@chem.helsinki.fi. E-mail: jonas.juselius@chem.uit.no. E-mail: ls.wang@pnl.gov.

10.1021/jp056789n CCC: $33.50 
Published on Web 03/08/2006

bimetallic $Cu_mLi_n$ ($m, n \leq 4$) clusters as well as the DFT studies by Tsipis et al.[20,21] who proposed a new class of molecules consisting of planar cyclic copper hydrides, $Cu_nH_n$.

In the present work, we report the generation of $Cu_4Na^-$ and $Au_4Na^-$ clusters in the gas phase and their characterization experimentally using photoelectron spectroscopy and computationally at correlated ab initio levels. The singly charged $M_4Li^-$ (M = Cu, Ag, Au) and $Ag_4Na^-$ species as well as the neutral $Cu_4Li_2$ and $Cu_4Na_2$ clusters have also been considered in the theoretical study. Photoelectron spectra of $Cu_4Na^-$ and $Au_4Na^-$ have been simulated by equation-of-motion coupled-cluster calculations of the low-lying electron detachment transitions and compared with the experimental data to identify the clusters observed in the PES experiment. The electron delocalization and aromaticity properties were studied by performing explicit calculations of the magnetically induced current densities using the newly developed GIMIC method.[16] Numerical integration of the magnetically induced current densities provided information about the ring-current strengths and the shape of the ring current. The GIMIC calculations clearly demonstrated that the square-planar coinage metal $M_4^{2-}$ clusters are $\sigma$-aromatic systems primarily due to the *s* orbital bonding.

## II. Experimental and Computational Methods

**A. Experimental Methods.** The experiments were carried out using a magnetic-bottle PES spectrometer, details of which have been described elsewhere.[22,23] Coinage-metal/sodium alloy clusters were produced by laser vaporization of compressed disk targets made from M (M = Cu, Au) and Na. The laser-produced plasma was mixed with a helium carrier gas pulse at 10 atm backing pressure. A cold cluster beam was produced by a supersonic expansion of the cluster/carrier gas mixture through a 2 mm diam nozzle and collimated by a 6 mm diam skimmer. The anions were extracted from the beam perpendicularly and separated by a time-of-flight mass spectrometer. The $M_4Na^-$ (M = Cu, Au) cluster anions of interest were selected and decelerated before crossing with a detachment laser beam in the interaction zone of the magnetic-bottle PES analyzer. Photoelectrons were collected at nearly 100% efficiency by the magnetic-bottle and analyzed in a 3.5-m long electron flight tube. The spectra were calibrated with the known spectra of $Cu^-$ and $Au^-$. The apparatus has an electron energy ($\Delta E/E$) resolution of ~2.5%, i.e., about 25 meV for photoelectrons of 1 eV kinetic energy.

**B. Computational Methods.** The molecular structures were optimized at the second-order Møller−Plesset perturbation level (MP2) using the TURBOMOLE program package.[24] The stationary points obtained in the structure optimizations were checked by calculating the vibrational frequencies numerically using finite differences. For Li, Na, Cu, and Ag, the Karlsruhe standard triple-$\zeta$ valence basis sets augmented with double polarization functions (TZVPP) were used. For gold, we employed the Karlsruhe Au basis set consisting of 7*s*5*p*3*d* basis functions[25] augmented with 2*f* as suggested by Pyykkö et al.[26] The 7*s*5*p*3*d* basis set has been optimized for the neutral gold trimer[25] and has proven to be cost efficient yielding accurate energies for gold species. Furche et al.[25] found that the addition of a *p* function with an exponent of about 0.8 is necessary for an accurate description of gold clusters.[27] For Ag and Au, the effective core potentials (ECP) from the Stuttgart group[28] were employed. The small-core ECP replaces 60 of the core electrons, and thus 19 electrons per gold atom were considered in the calculations. For Ag, also 19 electrons were considered thus replacing 28 core electrons with the ECP. In the correlation calculations on the $Cu_4^{2-}$ species, ten of the Cu electrons and two of the Na electrons were uncorrelated, whereas for the Ag and Au clusters all considered electrons were correlated. Single-point MP2 calculations using the Karlsruhe quadruple-$\zeta$ valence basis sets augmented with double sets of polarization functions (QZVPP) were employed to check the basis-set convergence of the isomer energy differences.

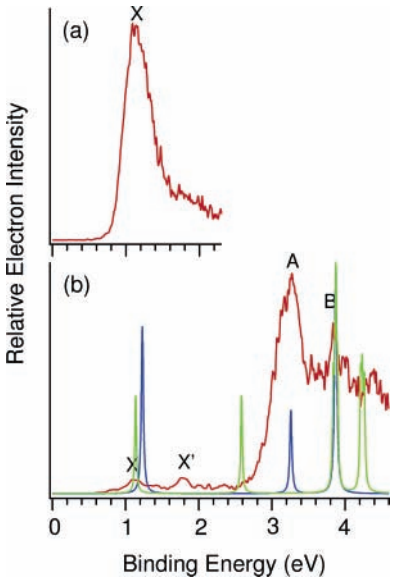


**Figure 1.** Comparison of calculated and measured photoelectron spectra of $Cu_4Na^-$. The measured spectra taken at (a) 532 nm (2.331 eV) and (b) 266 nm (4.661 eV) are shown in red. The calculated spectrum for the $C_{4v}$ isomer is shown in blue and the spectrum of the planar $C_{2v}$ isomer in green.

The photoelectron spectra were calculated at the coupled-cluster singles and doubles (CCSD) level using the equation-of-motion ionization-potential (EOMIP) formalism.[29] The coupled-cluster calculations were performed with the Austin-Mainz version of the ACES II program package.[30] The same basis sets as used in the structure optimizations were employed in the EOM calculations of the vertical detachment energies.

The nuclear magnetic shieldings and magnetically induced current densities for $Cu_4Li^-$ and $Cu_4Li_2$ were calculated at the CCSD level using ACES II.[31−34] The magnetically induced current densities were deduced from the one-particle density matrix, the magnetically perturbed density matrixes obtained in the shielding calculations, and basis-set information using the Gauge-Including Magnetically Induced Current (GIMIC) approach.[16] The GIMIC method has been described in detail in ref 16.

## III. Experimental Results

The measured photoelectron spectra of $Cu_4Na^-$ taken at two laser wavelengths, 532 nm (2.331 eV) and 266 nm (4.661 eV) are shown with the red curves in Figure 1. The photoelectron spectra of $Au_4Na^-$ recorded at three laser wavelengths are analogously shown in Figure 2. The 266 nm spectrum of $Cu_4Na^-$ displayed two weak bands (X, X′) at lower binding energies and two strong bands (A, B) at higher energies. The X′ band at 1.8 eV almost completely disappeared in the 532 nm spectrum and was most likely due to a mass contamination. The X band represents the transition from the ground state of $Cu_4Na^-$ to that of $Cu_4Na$, yielding adiabatic (ADE) and vertical (VDE) detachment energies of 0.83 and 1.13 eV, respectively. The broad peak of the X band suggests a significant geometry change between the ground states of $Cu_4Na^-$ and $Cu_4Na$. The

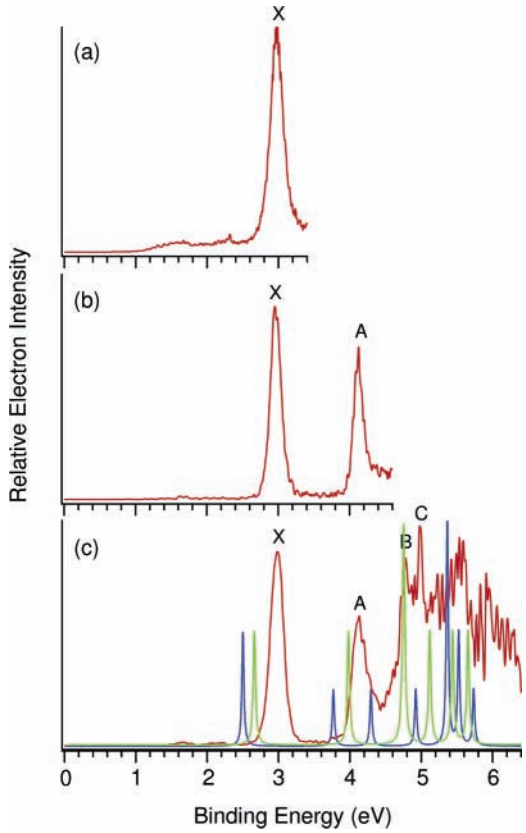


**Figure 2.** Comparison of calculated and measured photoelectron spectra of $Au_4Na^-$. The measured spectra taken at (a) 355 nm (3.496 eV), (b) 266 nm (4.661 eV), and (c) 193 nm (6.4244 eV) are shown in red. The calculated spectrum for the $C_{4v}$ isomer is shown in blue and the spectrum of the planar $C_{2v}$ isomer in green.

A band in Figure 1b corresponding to a VDE of 3.26 eV and the B band (VDE: 3.84 eV) represent detachment transitions to two excited states of $Cu_4Na$. Other weak features are also present on the higher binding energy side of the 266 nm spectrum, giving the congested appearance in this spectral range. The weak features are also most likely due to the contaminant associated with band X′.

The experimental photoelectron spectra of $Au_4Na^-$ in Figure 2 show no resemblance to those of $Cu_4Na^-$. $Au_4Na^-$ seems to have much higher electron binding energies. Its ground state transition defined by band X yielded ADE and VDE of 2.82 and 2.98 eV, respectively. Three excited state transitions (A, B, C) were clearly resolved at VDEs of 4.12, 4.79, and 4.98 eV, respectively. Higher binding energy features in the 193 nm spectrum were observed but not well resolved. The $Au_4Na^-$ spectra appear to have less contamination problems. The weak and broad features at lower binding energies (1.2 to 2.6 eV) in Figure 2a could be due to contamination or due to the presence of other low-lying isomers, but the 266 and 193 nm spectra shown in Figures 2b and 2c were quite clean.

The observed ADEs and VDEs are summarized in Table 1. To elucidate the structure and bonding of the two coinage alkali mixed clusters, the experimental data will be compared to calculated ionization potentials in Section 4.2.

## IV. Theoretical Results and Discussions

**A. Molecular Structures.** The energetically lowest structure obtained in the MP2/TZVPP optimization of $Cu_4Li_2$ is a bipyramidal cluster of $D_{4h}$ symmetry (Figure 3a). At this computational level, it lies 77.0 kJ/mol below the planar one

**TABLE 1: The Observed Vertical Electron Detachment Energies (VDE in eV) from the Photoelectron Spectra of $Cu_4Na^-$ in Figure 1 and $Au_4Na^-$ in Figure 2. the Uncertainty Is ± 0.05 eV**

| species | X[a] | A | B | C |
|---|---|---|---|---|
| $Cu_4Na^-$ | 1.13 | 3.26 | 3.84 | |
| $Au_4Na^-$ | 2.98 | 4.12 | 4.79 | 4.98 |

[a] The adiabatic detachment energies for the X band or the electron affinities for the corresponding neutral $Cu_4Na$ and $Au_4Na$ are measured as 0.83 ± 0.04 and 2.82 ± 0.04 eV, respectively.

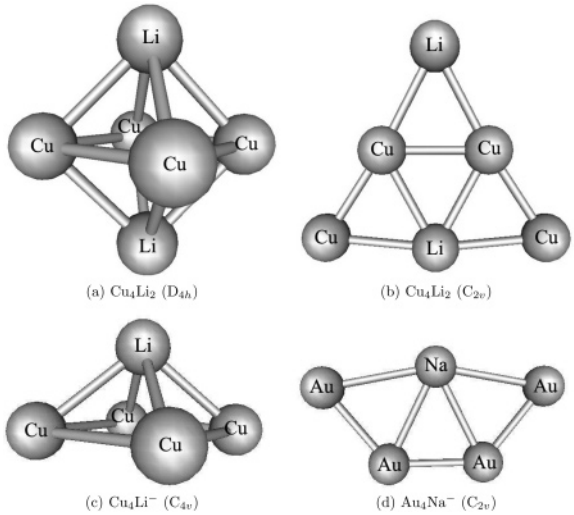


**Figure 3.** The molecular structure of (a) $Cu_4Li_2$ ($D_{4h}$), (b) $Cu_4Li_2$ ($C_{2v}$), (c) $Cu_4Li^-$ ($C_{4v}$), and (d) $Au_4Na^-$ ($C_{2v}$) optimized at the MP2 level using TZVPP (Cu, Li, Na) and 7*s*5*d*3*d*2*f* (Au) basis sets. The pictures have been made using gOpenMol.[43,44]

of $C_{2v}$ symmetry (Figure 3b). The Cu atoms in $Cu_4Li_2$ seems to prefer to form a square with equidistant Cu−Cu bonds as previously reported.[18]

At the MP2/TZVPP level, the singly charged $Cu_4Li^-$ cluster of $C_{4v}$ in Figure 3c is found to be 11.7 kJ/mol below the planar $C_{2v}$ isomer. The corresponding $Au_4Na^-$ isomer of $C_{2v}$ symmetry is shown in Figure 3d. However, the energy difference is small and by changing the counterion from $Li^+$ to $Na^+$ the pyramidal $C_{4v}$ and the planar $C_{2v}$ structures become almost degenerate with the planar structure 3.3 kJ/mol below the $C_{4v}$ one. The planar isomer is stabilized further by inclusion of higher-order electron correlation effects. In single-point CCSD/TZVPP and CCSD(T)/TZVPP calculations using the MP2/TZVPP structures, the planar isomer of $Cu_4Li^-$ is 16.4 and 3.1 kJ/mol below the pyramidal one. For $Cu_4Na^-$, the planar isomer is 3.4, 31.0, and 17.1 kJ/mol below the pyramidal structure calculated at the MP2, CCSD, and CCSD(T) levels. Zero-point energy corrections and entropy contributions do not change the order of the isomers since they reduce the energy difference between the planar and pyramidal isomers by only a few kJ/mol. However, at the MP2/QZVPP level the pyramidal $Cu_4Li^-$ and $Cu_4Na^-$ clusters are 45.7 and 30.2 kJ/mol below the planar isomers yielding extrapolated CCSD(T)/QZVPP isomer energies of 30.9 and 16.9 kJ/mol for $Cu_4Li^-$ and $Cu_4Na^-$, respectively. Thus, we conclude that for the singly charged $Cu_4Li^-$ and $Cu_4Na^-$ clusters, the pyramidal isomers of $C_{4v}$ symmetry are the energetically lowest ones.

The lowest isomer of $Cu_4Na_2$ is the bipyramidal cluster of $D_{4h}$ symmetry. At the MP2/TZVPP level it is found to be only 15.4 kJ/mol below the planar structure of $C_{2v}$ symmetry. As for $Cu_4Na^-$, the use of the QZVPP basis set favors the bipyramidal isomer, whereas high-order electron correlation

**TABLE 2: The Relative Isomer Energies (in kJ/mol) of the Planar ($C_{2v}$) $M_4A^-$ (M = Cu, Ag, and Au; A = Li and Na) Isomers Calculated at the MP2, CCSD, and CCSD(T) Levels Using the TZVPP (Li, Na, Cu, and Ag) and 7*s*5*p*3*d*2*f* (Au) Basis Sets[a]**

| species | MP2 | CCSD | CCSD(T) | CCSD(T)[b] |
|---|---|---|---|---|
| $Cu_4Li^-$ | 11.7 | −16.4 | −3.1 | 30.9 |
| $Cu_4Na^-$ | −3.5 | −31.0 | −17.1 | 16.9 |
| $Ag_4Li^-$ | 12.4 | −11.3 | −3.5 | − |
| $Ag_4Na^-$ | −3.0 | −28.0 | −18.8 | − |
| $Au_4Li^-$ | 0.6 | −41.3 | −29.7 | − |
| $Au_4Na^-$ | −17.9 | −63.1 | −49.4 | − |

[a] The molecular structures were optimized at the MP2 level using the same basis sets. Negative isomer energies indicate that the planar isomer is the lowest one. [b] Extrapolated CCSD(T)/QZVPP value.

contributions decrease the energy of the planar isomer relative to the bipyramidal one. At the extrapolated CCSD(T)/QZVPP level, the bipyramidal $Cu_4Li_2$ and $Cu_4Na_2$ clusters are found to be 99.8 and 54.5 kJ/mol below the planar ones.

The relative isomer energies of the $Ag_4^{2-}$ clusters are very similar to those of the corresponding Cu species. At the MP2/TZVPP level, pyramidal $Ag_4Li^-$ is 12.4 kJ/mol below the planar one, whereas at the CCSD/TZVPP and CCSD(T)/TZVPP levels, the planar isomer is 11.3 and 3.5 kJ/mol below the $C_{4v}$ structure. For the $Ag_4Na^-$ cluster, the MP2/TZVPP, CCSD/TZVPP, and CCSD(T)/TZVPP isomer energy differences are 3.0, 28.0, and 18.8 kJ/mol with the planar isomer below the pyramidal one. The use of QZVPP quality basis sets would most likely switch the order yielding the lowest energy for the pyramidal isomers as for the corresponding Cu clusters.

The $Au_4Li^-$ and $Au_4Na^-$ clusters were optimized at the MP2 level using the 7*s*5*p*3*d*2*f* basis set for Au and the TZVPP basis sets for Li and Na. At the MP2 level, the planar $Au_4Li^-$, isomer of $C_{2v}$ symmetry is only 0.6 kJ/mol above the pyramidal one, whereas CCSD and CCSD(T) calculations yielded the lowest energy for planar isomer. The isomer energy differences obtained at the CCSD and CCSD(T) levels are 41.3 and 29.7 kJ/mol. For $Au_4Na^-$, the planar isomer is significantly below the pyramidal structure at all computational levels. The isomer energy differences for $Au_4Na^-$ obtained at the MP2, CCSD, and CCSD(T) levels are 17.9, 63.1, and 49.4 kJ/mol. The lowest isomers of both $Au_4Li^-$ and $Au_4Na^-$ clusters are the planar ones. The energy differences between the planar and pyramidal isomers are so large that the use of larger basis sets would hardly change the order of them.

The relative isomer energies obtained at MP2, CCSD, and CCSD(T) levels are given in Table 2, and the bond distances obtained in the structure optimizations in Table 3. The optimized cluster structures of $Cu_4Li_2$ ($D_{4h}$), $Cu_4Li_2$ ($C_{2v}$), $Cu_4Li^-$ ($C_{4v}$), and $Au_4Na^-$ ($C_{2v}$) are shown in Figures 3a−d.

**B. Comparison Between Experimental and Calculated Photoelectron Spectra.** The simulated photoelectron spectra of the pyramidal and planar $Cu_4Na^-$ clusters shown as the blue and green curves in Figure 1 were calculated at the EOMIP CCSD level. The obtained VDEs for the pyramidal ($C_{4v}$) $Cu_4Li^-$ and $Cu_4Na^-$ clusters as well as the planar ($C_{2v}$) $Cu_4Na^-$ cluster are given in Table 4. The calculated photoelectron spectra are rather independent of whether $Li^+$ or $Na^+$ is used as counterion, whereas the spectra for the planar and pyramidal $Cu_4Na^-$ isomers differ significantly. The calculated spectra of the pyramidal $Cu_4Li^-$ and $Cu_4Na^-$ are very similar, except for the fourth detachment channel (Table 4). However, the peak patterns of the calculated spectra of the planar and pyramidal $Cu_4Na^-$ clusters are completely different. This structural sensitivity of photoelectron spectra provides the basis for using PES and

**TABLE 3: The M−M and M−A Bond Distances (in pm) of the $M_4A^-$ and $M_4A_2$ Species (M = Cu, Ag, and Au; A = Li and Na) Optimized at the MP2 Level Using the TZVPP (Li, Na, Cu, Ag) and 7*s*5*p*3*d*2*f* (Au) Basis Sets**

| species | level | symmetry | M−M[a] | M−M[b] | M−A[c] | M−A[d] |
|---|---|---|---|---|---|---|
| $Cu_4Li^-$ | MP2/TZVPP | $C_{4v}$ | 242.0 | | 240.3 | |
| $Cu_4Na^-$ | MP2/TZVPP[e] | $C_{4v}$ | 242.0 | | 275.0 | |
| $Cu_4Li^-$ | MP2/TZVPP | $C_{2v}$ | 243.6 | 235.8 | 248.5 | 244.5 |
| $Cu_4Na^-$ | MP2/TZVPP | $C_{2v}$ | 244.2 | 236.0 | 280.0 | 284.8 |
| $Ag_4Li^-$ | MP2/TZVPP | $C_{4v}$ | 270.6 | | 253.6 | |
| $Ag_4Na^-$ | MP2/TZVPP | $C_{4v}$ | 270.1 | | 288.9 | |
| $Ag_4Li^-$ | MP2/TZVPP | $C_{2v}$ | 269.6 | 260.6 | 260.8 | 261.7 |
| $Ag_4Na^-$ | MP2/TZVPP | $C_{2v}$ | 270.3 | 260.3 | 292.2 | 300.0 |
| $Au_4Li^-$ | MP2/7*s*5*p*3*d*2*f* | $C_{4v}$ | 264.3 | | 249.1 | |
| $Au_4Na^-$ | MP2/7*s*5*p*3*d*2*f* | $C_{4v}$ | 263.6 | | 282.3 | |
| $Au_4Li^-$ | MP2/7*s*5*p*3*d*2*f* | $C_{2v}$ | 261.1 | 251.4 | 257.5 | 255.7 |
| $Au_4Na^-$ | MP2/7*s*5*p*3*d*2*f* | $C_{2v}$ | 260.9 | 251.1 | 294.5 | 284.4 |
| $Cu_4Li_2$ | MP2/TZVPP | $D_{4h}$ | 246.1 | | 242.8 | |
| $Cu_4Na_2$ | MP2/TZVPP | $D_{4v}$ | 243.8 | | 280.8 | |
| $Cu_4Li_2$ | MP2/TZVPP | $C_{2v}$[f] | 237.4 | 237.8 | 250.1 | 251.8 |
| $Cu_4Na_2$ | MP2/TZVPP | $C_{2v}$[g] | 237.7 | 239.3 | 282.1 | 290.0 |

[a] For the planar clusters of $C_{2v}$ symmetry, the distance between the inner and outer M atoms. [b] The distance between the two inner M atoms of the planar clusters. [c] For the planar clusters of $C_{2v}$ symmetry, the distance between the A atom and the outer M atom of the planar clusters. [d] The distance between the A atom and the inner M atom of the planar clusters. [e] The corresponding distances obtained at the CCSD/TZVPP level are 251.7 and 280.4 pm. [f] The distance between the inner Cu atom and the Li atom at the cusp is 255.0 pm. [g] The distance between the inner Cu atom and the Na atom at the cusp is 282.0 pm.

**TABLE 4: The Vertical Detachment Energies (VDE in eV) for $Cu_4Li^-$, $Cu_4Na^-$, and $Au_4Na^-$ Calculated at the EOMIP CCSD Level as Compared to Experimental Data[a]**

| $Cu_4Li^-$ | $Cu_4Na^-$ | | | $Au_4Na^-$ | | |
|---|---|---|---|---|---|---|
| calcd | calcd | | | calcd | | |
| ($C_{4v}$) | ($C_{4v}$) | ($C_{2v}$) | exp | ($C_{4v}$) | ($C_{2v}$) | exp |
| 1.313 | 1.229 | 1.137 | 1.13 | 2.501 | 2.662 | 2.98 |
| 3.193 | 3.259 | 2.586 | 3.26 | 3.769 | 3.980 | 4.12 |
| 3.636 | 3.864 | 3.840 | 3.84 | 4.295 | 4.751 | 4.79 |
| 4.062 | 3.876 | 3.871 | | 4.923 | 4.758 | 4.98 |
| | | 3.985 | | 5.365 | 5.120 | |
| | | 4.213 | | 5.525 | 5.439 | |
| | | | | 5.734 | 5.656 | |

[a] The molecular structures optimized at the MP2 level were used. The cluster symmetry is also indicated

calculations to determine cluster structures. We were not able to measure the photoelectron spectra of $Cu_4Li^-$ because of its complicated isotope pattern. Our measured photoelectron spectra of $Cu_4Na^-$ (the red curves in Figure 1) are in good agreement with the simulated spectrum for the pyramidal structure (the blue curve) but disagree with the simulated spectrum for the planar structure (the green curve). In particular, the second detachment channel for the planar structure with a calculated VDE at 2.586 eV has no corresponding peak in the experimental spectrum. The comparison between the calculated and measured photoelectron spectra suggests that the experimental spectra are due to the $Cu_4Na^-$ cluster of $C_{4v}$ symmetry, consisting of a planar four-membered $Cu_4^{2-}$ ring. The planar $Cu_4Na^-$ isomer of $C_{2v}$ symmetry can be ruled out to be the main contributor to the experimental spectra since its second VDE deviates by 0.66 eV from the experimental value (Table 4) and the estimated uncertainty of the VDE calculated at the EOMIP CCSD/TZVPP level is significantly smaller.[35]

The calculated photoelectron spectra of the planar ($C_{2v}$) and pyramidal ($C_{4v}$) isomers of $Au_4Na^-$ at the EOMIP CCSD level


**Figure 4.** The HOMO (a) and HOMO-1 (b) molecular orbitals of $Cu_4Li_2$ calculated at the Hartree−Fock self-consistent field (HF SCF/TZVPP) level using the MP2/TZVPP molecular structure. The orbitals are spectated along the $C_4$ axis. The orbital energies (in eV) are given within parentheses. The pictures have been made using gOpenMol [43,-44].

are shown in Figure 2, and the obtained ionization potentials are compared with the experimental VDEs in Table 4. Clearly, the calculated spectral pattern of the planar isomer (the green curve in Figure 2) agrees well with the experimental spectra (the red curves), although the calculated VDEs are somewhat smaller than the observed ones (Table 4). On the other hand, the pattern of the calculated photoelectron spectra for the pyramidal $Au_4Na^-$ cluster (the blue curve in Figure 2) differs significantly from that of the experimental spectrum. These observations are consistent with the energetics of the two $Au_4Na^-$ isomers and confirm that the planar $Au_4Na^-$ isomer is indeed the global minimum.

**C. The Nature of the Aromaticity of the Square-Planar $Cu_4^{2-}$ Unit.** Wannere et al.[18] calculated nucleus independent chemical shifts (NICS) for bipyramidal $Cu_4Li_2$, $Ag_4Li_2$, and $Au_4Li_2$. On the basis of the NICS contributions from different orbitals, they concluded that the aromatic properties of these clusters possess distinct differences from other square ring systems such as $Al_4Li_2$. According to their NICS calculations, the coinage four-membered rings are stabilized by *d* orbital aromaticity i.e., the cyclic electron delocalization is due to *d* electrons rather than *p* electrons as in ordinary aromatic molecules, because they found that the diamagnetic NICS value of −14.5 ppm at the center of the cluster seems to originate from MOs with significant 3*d* character. The self-canceling orbital contributions in the NICS treatment is probably an artifact due to an unphysical orbital decomposition.[36] A comparison of the nuclear magnetic shielding constants for the Cu atoms, $\sigma$(Cu), calculated at ab initio and DFT levels of theory also indicates that generalized gradient (GGA) DFT methods should not be used to assess the aromaticity properties of the $Cu_4^{2-}$ species. Calculations of the nuclear magnetic shielding constants ($\sigma$) for $Cu_4Li_2$ at the DFT level using Becke's three-parameter hybrid functional (B3LYP)[37,38] yield $\sigma$(Cu) values which are 600 ppm (67%) larger than the shielding constants obtained at the BP86 GGA level.[39−41] The $\sigma$(Cu) values calculated at the HF/TZVPP, MP2/TZVPP, and CCSD/TZVPP levels are 1838, 1675, and 1690 ppm, respectively, as compared to the B3LYP/TZVPP and BP86/TZVPP values of 1473 and 881 ppm. The small $\sigma$(Cu) value obtained in the BP86 GGA DFT calculation indicates that GGA DFT calculations are not recommended for studies of the magnetic shieldings of the $Cu_4^{2-}$ clusters, whereas the Hartree-Fock-based ab initio correlation methods (MP2 and CCSD) seem to yield consistent nuclear magnetic shieldings.

The orbital plot in Figure 4 shows that the $a_{1g}$ orbital has a large amplitude at the center of the $Cu_4Li_2$ cluster. The presence of a significant amount of electron charge at the cluster center shields the external magnetic field in the NICS point. Thus, the diamagnetic shielding contribution from the $a_{1g}$ orbital in the NICS point is due to the presence of its electrons and not due to ring currents sustained by it. However, the highest occupied molecular orbital (HOMO) belonging to the $e_u$ irreducible representation is ring-shaped and has a significant amplitude outside the $Cu_4^{2-}$ ring. The orbital pictures suggest that the HOMO is sustaining the current and therefore responsible for the aromaticity properties of the $Cu_4^{2-}$ ring.

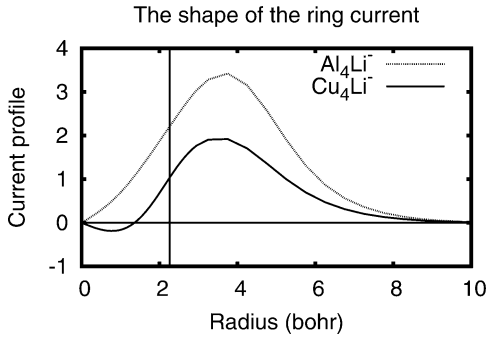


**Figure 5.** The shape of the ring current (in nA/T/bohr) for $Cu_4Li^-$ calculated at the CCSD/TZVPP level using the MP2/TZVPP molecular structure is compared to the ring current profile of the $Al_4^{2-}$ ring [14]. The vertical bar denotes the size of the $Cu_4^{2-}$ ring. The size of the $Al_4^{2-}$ ring is 0.2 bohr greater.

**TABLE 5: The Integrated Ring-Current Susceptibilities (in nA/T) for $Cu_4Li^-$, $Cu_4Li_2$, and $Cu_4H_4$ Calculated at the CCSD/TZVPP Level Using the GIMIC Method**

| | $Al_4Li^-$ [a] | $Cu_4Li^-$ | $Cu_4Li_2$ | $Cu_4H_4$ |
|---|---|---|---|---|
| diamagnetic current | 32.4 | 19.4 | 23.2 | 2.1 |
| paramagnetic current | 0.0 | −0.4 | −0.4 | −2.7 |
| total current | 32.4 | 19.0 | 22.8 | −0.6 |
| contribution from Li[b] | 4.3 | 6.4 | 12.9 | − |
| total ring current | 28.1 | 12.6 | 10.0 | −0.6 |

[a] From ref 14. [b] The estimated net current circling the $Li^+$ cations.

The first-order magnetically induced current density for $Cu_4Li^-$ was calculated at the CCSD/TZVPP level using the GIMIC method.[16] In Figure 5, the shape of the magnetically induced ring current passing on the open side of the $Cu_4Li^-$ ring is compared to the corresponding curve for $Al_4Li^-$. The current profiles of the two species are strikingly similar. The main difference between the $Cu_4^{2-}$ and $Al_4^{2-}$ currents is that for $Cu_4^{2-}$ the current in the interior of the molecular ring is weak and dominantly paramagnetic, whereas for $Al_4^{2-}$ the ring current is diatropic both inside and outside the ring. The $a_{1g}$ orbital (HOMO-1) of $Cu_4Li^-$ which has large amplitudes inside the ring does apparently not sustain any strong ring current. The large ring current appearing outside the $Cu_4^{2-}$ ring suggests that the $e_u$ orbital (HOMO) is mainly responsible for the transport of the electrons.

The integrated ring-current strengths passing a radial cross section are given in Table 5. The ring-current susceptibilities of 12.6 and 10.0 nA/T for $Cu_4Li^-$ and $Cu_4Li_2$, respectively, are about as large as in benzene.[16,42] The ring-current susceptibility of the $Cu_4^{2-}$ ring is thus 2−3 times weaker than for the $Al_4^{2-}$ species.

The explicit orbital contributions to the magnetically induced currents cannot be obtained using the GIMIC method, because orbital currents are dependent on the choice of the gauge origin[36] and the unphysical current contributions from mixing of occupied orbitals cannot be eliminated in the GIMIC scheme. The contribution from valence *s* orbitals was therefore estimated by removing them from the basis set. In the current calculations without valence *s* orbitals, the ring-current susceptibility obtained at the MP2 level is 4.0 nA/T as compared to the MP2/TZVPP value of 12.2 nA/T; the $Cu_4^{2-}$ ring sustains a weak ring current when the valence *s* basis functions are absent.

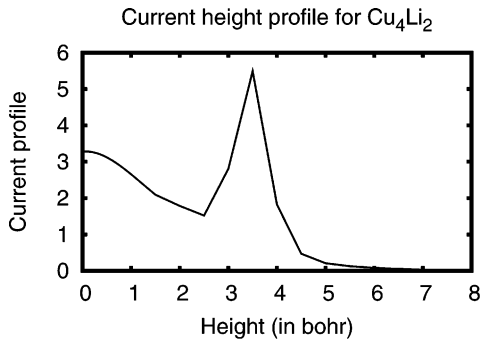


**Figure 6.** The current profile (in nA/T/bohr) as a function of the vertical distance from the $Cu_4^{2-}$ ring in $Cu_4Li_2$ calculated at the CCSD/TZVPP level using the MP2/TZVPP structure.

The GIMIC calculation of the vertical current profile in Figure 6 shows that the current in $Cu_4Li_2$ is not only sustained in the ring plane, but also between the ring and the $Li^+$ counterions. The sharp peak at 3.5 bohr is due to the $Li^+$ cations. The GIMIC calculations of the current density of $Cu_4Li^-$ show that $Cu_4^{2-}$ can be considered to be $\sigma$ aromatic. In contrast to Wannere et al.,[18] we find no need to invoke the *d*-orbitals in order to explain the aromaticity of planar four-membered $Cu_4^{2-}$ rings. In the case of $Au_4Na^-$, the calculations show that the planar isomer of $C_{2v}$ symmetry is the energetically lowest one. This is also in agreement with experiment, since the measured photoelectron spectra indicates that the planar $Au_4Na^-$ is also observed experimentally.

The magnetically induced current density was also calculated for $Cu_4H_4$, which is a planar molecule consisting of a square-shaped $Cu_4$ ring with the hydrogens bridging around it at the edges. As seen in Table 5, the $Cu_4$ ring in $Cu_4H_4$ does not sustain any strong magnetically induced ring current. The weak diatropic current circles inside and outside the $Cu_4$ ring, whereas the region in the vicinity of the H atoms and outside them are dominated by the paratropic ring current. The net ring-current susceptibility for $Cu_4H_4$ is only $-0.6$ nA/T.

## V. Conclusions

Two coinage and alkali metal mixed clusters ($Cu_4Na^-$ and $Au_4Na^-$) produced with laser vaporization have been characterized experimentally using photoelectron spectroscopy and computationally at correlated ab initio levels. The comparison of measured and calculated photoelectron spectra shows that the observed $Cu_4Na^-$ cluster is a pyramidal species with $C_{4v}$ symmetry, whereas the observed $Au_4Na^-$ cluster is planar with $C_{2v}$ symmetry.

Ab initio electron correlation calculations also predict the pyramidal $Cu_4Na^-$ and the planar $Au_4Na^-$ isomers to be the energetically lowest ones. At the CCSD(T)/7*s*5*p*3*d*2*f* level, the planar $Au_4Na^-$ isomer lies 49.4 kJ/mol below the pyramidal one, whereas at extrapolated CCSD(T)/QZVPP level, the pyramidal $Cu_4Na^-$ cluster lies 16.9 kJ/mol below the planar one. Ab initio calculations on $Ag_4Li^-$ and $Ag_4Na^-$ show that the energetics of the $Ag_4^{2-}$ clusters are similar to those of the $Cu_4^{2-}$ species. The pyramidal $Ag_4Li^-$ and $Ag_4Na^-$ clusters are thus most likely the global minima.

Calculations of the magnetically induced current density in pyramidal $Cu_4Li^-$ ($C_{4v}$) and bipyramidal $Cu_4Li_2$ ($D_{4h}$) clusters using the Gauge-Including Magnetically Induced Current (GIMIC) method show that the strong ring current is sustained mainly by the highest-occupied molecular orbital dominated by Cu 4*s* character. The $Cu_4^{2-}$ ring is $\sigma$ aromatic mainly from the 4*s* bonding interactions and the *d* orbitals do not sustain any strong ring current. The aromatic character of $Cu_4^{2-}$ can thus be explained in terms of $\sigma$ aromaticity. We found no evidence of any significant current density being sustained by the *d*-orbitals.

**Acknowledgment.** We acknowledge financial support from the European research training network on "Understanding Nanomaterials from a Quantum Perspective" (NANOQUANT), contract No. MRTN-CT-2003-506842, from the Nordisk Forskerakademi network for research and research training (NorFA grant No. 030262) on "Quantum Modeling of Molecular Materials" (QMMM), from The Academy of Finland (FA projects 53915, 200903, and 206102), and from Magnus Ehrnrooth's Foundation. We also thank Prof. Reinhart Ahlrichs (Karlsruhe) and Prof. Jürgen Gauss (Mainz) for up-to-date versions of the TURBOMOLE and ACES II program packages. The experimental work was supported by the US National Science Foundation (DMR-0503383) and performed at the W.R. Wiley Environmental Molecular Sciences Laboratory, a national scientific user facility sponsored by the US DOE's Office of Biological and Environmental Research and located at Pacific Northwest National Laboratory, operated for the DOE by Battelle.

**Supporting Information Available:** The atomic coordinates are given for the molecular structures of $Cu_4Li^-$, $Cu_4Na^-$, $Ag_4Li^-$, $Ag_4Na^-$, $Au_4Li^-$, $Au_4Na^-$, $Cu_4Li_2$, $Cu_4Na_2$, $Ag_4Li_2$, $Ag_4Na_2$, $Au_4Li_2$, and $Au_4Na_2$ optimized at the MP2 level using the TZVPP (Cu, Ag, Li, and Na) and 7*s*5*d*3*d*2*f* (Au) basis sets. The total energies (in a.u.) calculated at HF, MP2, CCSD, and CCSD(T) levels are also reported. This material is available free of charge via the Internet at http://pubs.acs.org.

## References and Notes

(1) Li, X.; Kuznetsov, A. E.; Zhang, H. F.; Boldyrev, A. I.; Wang, L. S. *Science* **2001**, *291*, 859.

(2) Kuznetsov, A. E.; Birch, K. A.; Boldyrev, A. I.; Li, X.; Zhai, H. J.; Wang, L. S. *Science* **2003**, *300*, 622.

(3) Kuznetsov, A. E.; Corbett, J. D.; Wang, L. S.; Boldyrev, A. I. *Angew. Chem., Int. Ed.* **2001**, *40*, 3369.

(4) Boldyrev, A. I.; Kuznetsov, A. E. *Inorg. Chem.* **2002**, *41*, 532.

(5) Kuznetsov, A. E.; Boldyrev, A. I.; Li, X.; Wang, L. S. *J. Am. Chem. Soc.* **2001**, *123*, 8825.

(6) Li, X.; Zhang, H. F.; Wang, L. S.; Kuznetsov, A. E.; Cannon, N. A.; Boldyrev, A. I. *Angew. Chem., Int. Ed.* **2001**, *40*, 1867.

(7) Boldyrev, A. I.; Wang, L. S. *Chem. Rev.* **2005**, *105*, 3716.

(8) Heine, T.; Corminboeuf, C.; Seifert, G. *Chem. Rev.* **2005**, *105*, 3889.

(9) Jusélius, J.; Straka, M.; Sundholm, D. *J. Phys. Chem. A* **2001**, *105*, 9939.

(10) Fowler, P. W.; Havenith, R. W. A.; Steiner, E. *Chem. Phys. Lett.* **2001**, *342*, 85.

(11) Zhan, C.-G.; Zheng, F.; Dixon, D. A. *J. Am. Chem. Soc.* **2002**, *124*, 14795.

(12) Chen, Z.; Corminboeuf, C.; Heine, T.; Bohmann, J.; von Ragué Schleyer, P. *J. Am. Chem. Soc.* **2003**, *125*, 13930.

(13) Havenith, R. W. A.; Fowler, P. W.; Steiner, E.; Shetty, S.; Kanhere, D.; Pal, S. *Phys. Chem. Chem. Phys.* **2004**, *6*, 285.

(14) Lin, Y. C.; Jusélius, J.; Sundholm, D.; Gauss, J. *J. Chem. Phys.* **2005**, *122*, 214308.

(15) von Ragué Schleyer, P.; Maerker, C.; Dransfeld, A.; Jiao, H.; van Eikema Hommes, N. J. R. *J. Am. Chem. Soc.* **1996**, *118*, 6317.

(16) Jusélius, J.; Sundholm, D.; Gauss, J. *J. Chem. Phys.* **2004**, *121*, 3952.

(17) Ritter, S. K. *Chem. Eng. News* **2003**, *81* (50), 23.

(18) Wannere, C. S.; Corminboeuf, C.; Wang, Z. X.; Wodrich, M. D.; King, R. B.; von Ragué Schleyer, P. *J. Am. Chem. Soc.* **2005**, *127*, 5701.

(19) Fuentealba, P.; Padilla-Campos, L. *Intern. J. Quantum Chem.* **2005**, *102*, 498.

(20) Tsipis, A. C.; Tsipis, C. A. *J. Am. Chem. Soc.* **2003**, *125*, 1136.

(21) Tsipis, A. C.; Karagiannis, E. E.; Kladou, P. F.; Tsipis, C. A. *J. Am. Chem. Soc.* **2004**, *126*, 12916.

(22) Wang, L. S.; Cheng, H. S.; Fan, J. *J. Chem. Phys.* **1995**, *102*, 9480.

(23) Wang, L. S.; Wu, H. in *Advances in Metal and Semiconductor Clusters: Cluster Materials*; Duncan, M. A., Ed.; JAI Press: Greenwich, CT, 1998; pp 299−343.
(24) Ahlrichs, R.; Bär, M.; Häser, M.; Horn, H.; Kölmel, C. *Chem. Phys. Lett.* **1989**, *162*, 165, current version: see http://www.turbomole.de.
(25) Gilb, S.; Weis, P.; Furche, F.; Ahlrichs, R.; Kappes, M. M. *J. Chem. Phys.* **2002**, *116*, 4094.
(26) Pyykkö, P.; Runeberg, N.; Mendizabal, F. *Chem. Eur. J.* **1997**, *3*, 1451.
(27) The optimized *p* exponent of 0.80896058156 was used. The exponents of the *f* functions were 1.19 and 0.43023309776.[25]
(28) Andrae, D.; Häussermann, U.; Dolg, M.; Stoll, H.; Preuss, H. *Theor. Chim. Acta* **1990**, *77*, 123.
(29) Stanton, J. F. *J. Chem. Phys.* **1994**, *101*, 8938.
(30) Stanton, J. F.; Gauss, J.; Watts, J. D.; Lauderdale, W. J.; Bartlett, R. J. *Intern. J. Quantum Chem. Symp.* **1992**, *26*, 879, current version: see http://www.aces2.de.
(31) Gauss, J. *Chem. Phys. Lett.* **1992**, *191*, 614.
(32) Gauss, J. *J. Chem. Phys.* **1993**, *99*, 3629.
(33) Gauss, J.; Stanton, J. F. *J. Chem. Phys.* **1995a**, *102*, 251.
(34) Gauss, J.; Stanton, J. F. *J. Chem. Phys.* **1995b**, *103*, 3561.
(35) Stanton, J. F.; Sattelmeyer, K. W.; Gauss, J.; Allan, M.; Skalicky, T.; Bally, T. *J. Chem. Phys.* **2001**, *115*, 1.
(36) Steiner, E.; Fowler, P. W. *Phys. Chem. Chem. Phys.* **2004**, *6*, 261.
(37) Becke, A. D. *J. Chem. Phys.* **1993**, *98*, 5648.
(38) Lee, C.; Yang, W.; Parr, R. G. *Phys. Rev. B* **1988**, *37*, 785.
(39) Vosko, S. H.; Wilk, L.; Nusair, M. *Can. J. Phys* **1980**, *58*, 1200.
(40) Perdew, J. P. *Phys. Rev. B* **1986**, *33*, 8822.
(41) Becke, A. D. *Phys. Rev. A* **1988**, *38*, 3098.
(42) Johansson, M. P.; Jusélius, J.; Sundholm, D. *Angew. Chem., Int. Ed.* **2005**, *44*, 1843.
(43) Laaksonen, L. *J. Mol. Graphics* **1992**, *10*, 33, current version: see http://www.csc.fi/gopenmol.
(44) Bergman, D. L.; Laaksonen, L.; Laaksonen, A. *J. Mol. Graphics Modell.* **1997**, *15*, 301.